Environmental Science and Pollution Research
https://doi.org/10.1007/s11356-025-37358-4

RESEARCH ARTICLE

Iron-modified barley straw biochar for nitrate and phosphate removal from water

Sepideh Ansari[1,2] · **Ricardo Bello-Mendoza**[1] · **Aisling O'Sullivan**[1,2]

Received: 12 September 2025 / Accepted: 19 December 2025

Abstract

Excessive nitrate and phosphate in water pose serious environmental and health risks, requiring effective and sustainable removal methods. This study investigates the efficiency of iron-modified biochar derived from barley straw (Fe-BSBC) for removing these pollutants from water. The influence of contact time, pH, adsorbent dosage, and competing anions on adsorption performance was tested in batch experiments. At pH 6 and 23 ± 1 °C, with an initial adsorbate concentration of 15 mg/L and adsorbent dosages of 5 g/L for phosphate and 15 g/L for nitrate, equilibrium was achieved within 8 h for phosphate and 24 h for nitrate. Fe-BSBC demonstrated adsorption capacities of 13.7 mg/g for phosphate and 2.0 mg/g for nitrate, outperforming most of the previously reported biochar adsorbents. Isotherm modelling indicated that the Sips model best described the adsorption process, suggesting multilayer and heterogeneous adsorption. Predicted maximum adsorption capacities were 22.0 mg/g for phosphate and 4.07 mg/g for nitrate. Kinetic data aligned with the pseudo-second-order model, indicating chemisorption as the primary mechanism. Electrostatic attraction was identified as the main mechanism for nitrate adsorption, evidenced by a decrease in zeta potential after nitrate uptake and supported by FTIR, EDS, and XRD characterisation. Conversely, phosphate removal was mainly driven by ligand exchange, leading to the formation of Fe–O–P complexes, alongside electrostatic interactions. Overall, Fe-BSBC presents a cost-effective and scalable water treatment solution that supports the Sustainable Development Goals.

Keywords Adsorption · Agricultural waste · Metal modification · Nitrogen · Nutrients · Phosphorus · Water treatment

Introduction

Water quality degradation caused by excessive nutrients (nitrate and phosphate) in water bodies due to discharges of inadequately treated runoff and wastewater has become a global problem. This issue negatively impacts ecosystems, biodiversity, drinking water security, and ultimately, the well-being of people (Hashemi et al. 2016; Cai and Ye 2022). Excessive phosphate concentrations lead to eutrophication, which reduces dissolved oxygen levels in water bodies (Nijboer and Verdonschot 2004). Likewise, elevated nitrate concentrations in drinking water can cause methemoglobinemia (or blue baby syndrome), various types of cancers, enlargement of the thyroid gland, diabetes, and adverse reproductive outcomes (Ward 2009). Effective and practical treatment methods are needed to address this water pollution problem.

Adsorption is one of the most promising methods for nutrient removal from water due to its low cost, high efficiency, and ease of operation and maintenance (Anastopoulos et al. 2017). Recently, the use of biochar produced from biowaste and agricultural residues as an adsorbent has attracted the attention of researchers and practitioners. Biochar has exceptional adsorption and ion-exchange capacities due to its porous structure, extensive specific surface area, and carboxyl functional groups (Inyang et al. 2016). In many parts of the world, agricultural waste is burned at source, causing air pollution and chronic health effects (Jones et al. 2023). Converting these waste materials into biochar not

Responsible Editor: Zhihong Xu

✉ Ricardo Bello-Mendoza
ricardo.bellomendoza@canterbury.ac.nz

[1] Department of Civil and Environmental Engineering, University of Canterbury, Private Bag, 4800, Christchurch 8140, New Zealand

[2] Centre for Ecological Technical Solutions (CELTS), University of Canterbury, Private Bag 4800, Christchurch 8140, New Zealand

Published online: 27 January 2026

only adds commercial value but also helps mitigate the significant disposal challenges associated with them. However, most biochar types possess a net negative surface charge, which limits their effectiveness in adsorbing anionic pollutants (Deng et al. 2021).

Incorporating iron (Fe) onto the biochar surface can increase its positive surface charge, thereby improving its electrostatic attraction and anion exchange capacity (Ou et al. 2023). The Fe ions attached to the biochar surface can efficiently interact with anions such as NO_3^- and PO_4^{3-}, thereby enhancing the removal of these anionic pollutants (Inyang et al. 2010). Iron (hydr)oxide adsorbents have been investigated for phosphate removal from aqueous solutions due to their abundance, chemical stability in oxygenated waters, cost-effectiveness, and environmentally friendly nature (Liu et al. 2018). Perera et al. (2024) synthesized iron-functionalized pine woodchips and iron-functionalized commercial biochar derived from woodchips for phosphate removal from agricultural drainage, demonstrating high phosphate adsorption. Similarly, Long et al. (2019) utilized $FeCl_3$ to modify corncob biochar, thereby enhancing its positively charged surface for nitrate removal. Batch experiments showed that nitrate adsorption on iron-modified biochar remained stable across a range of pH and temperature values, with a maximum adsorption capacity of 32.33 mg/g. Other studies have investigated iron-modified biochar derived from various biowaste sources, such as corn straw (Liu et al. 2015), bamboo (Ou et al. 2023), and reed waste (Kuang et al. 2023), waste Douglas fir (Dewage et al. 2018) and mangrove green waste (Usman et al. 2016) for either nitrate or phosphate removal. The evaluation of iron-modified biochar's efficiency in removing both phosphate and nitrate remains largely unaddressed in the literature, despite these two pollutants being commonly found together in impacted water bodies or in wastewater.

Among the various biowaste resources used to produce biochar, barley straw (BS) remains unexplored for nitrate and phosphate removal despite its promising characteristics and abundance. According to the FAO (2023), barley (*Hordeum vulgare* L.) was among the five most produced cereal species globally in 2022, with 155 million tonnes produced that year. Barley is primarily used to produce malt, in animal feed, and in human nutrition. The growing and processing of barley generates a significant amount of waste, mainly comprising straw (Garcia-Garcia and Rahimifard 2019). Barley straw is used for energy production and as fodder, but a significant amount is not utilized and is discarded as waste (Zhu et al. 2015). Therefore, using barley straw as a promising renewable resource for producing adsorbents for nutrient removal would be advantageous from both environmental and economic perspectives.

The effectiveness of barley straw as an adsorbent in various forms for removing contaminants from water has been investigated due to its abundance, renewable nature, active functional groups, and high cellulosic composition (46% cellulose, 23% hemicellulose, and 15% lignin) (Ahmed et al. 2024; Zhu et al. 2015). The most widely studied pollutants treated with it include heavy metals such as cadmium and lead (Jazini et al. 2018); dyes such as methylene blue (Yue et al. 2024; Farouk et al. 2021) and malachite green (Ghasemi et al. 2020); antibiotics like levofloxacin (Yan et al. 2017) and norfloxacin (Yan and Niu 2018); and organic pollutants such as phenol (Maleki et al. 2010), oil (Ibrahim et al. 2010) and salicylic acid (Ahmed and Hameed 2018). In most of these studies, carbonaceous adsorbents derived from barley straw (biochar and activated carbon) or chemically modified barley straw were used. This is because most raw agricultural wastes, including raw barley straws, cannot be used in their original form (Mo et al. 2018) due to their inherently low mechanical stability. Therefore, thermal or chemical modifications (e.g., pyrolysis, crosslinking, and functionalization) are necessary to improve porosity, surface area, and functional groups, enhancing their adsorption capacity.

Despite considerable prior research, no studies have explored the potential use of biochar derived from barley straw for phosphate and nitrate removal from aqueous solutions. Also, as noted before, research on the use of iron-modified biochar from different agricultural wastes has focused on either phosphate or nitrate removal, even though these two pollutants are often found together in contaminated water. Furthermore, the nutrient adsorption capacity of biochar remains relatively low. For example, the highest phosphate adsorption capacity reported is 58.24 mg/g for bamboo-derived biochar modified with Fe and Ca and used to treat industrial wastewater (Ou et al. 2023). Phosphate concentrations as high as 200 mg/L were used, which doesn't reflect the concentrations found in most municipal wastewater or in the environment. A phosphate adsorption capacity of 23.33 mg/g was reported for iron-modified carbon at pH 2 (Delgadillo-Velasco et al. 2021). Still, the low pH requirement limits the adsorbent to low-scale applications, where the use of acids for pH control could be feasible.

Therefore, this study aims to produce iron-treated barley straw biochar (Fe-BSBC) and evaluate its effectiveness in simultaneously removing nitrate (NO_3^-) and phosphate (PO_4^{3-}) from water at concentrations and pH levels closer to those of most wastewater and contaminated water bodies. The nutrient removal capacity of the Fe-BSBC was examined through a series of batch adsorption experiments conducted under varying contact times, pH levels, adsorbent dosages, and in the presence of competing anions. The kinetics and isotherm characteristics of nitrate and phosphate uptake were analyzed, and the adsorbent was characterized using standard microscopic and spectroscopic techniques.

Materials and methods

Chemicals and materials

Ferric chloride ($FeCl_3 \cdot 6H_2O$), sodium chloride (NaCl), ammonium hydroxide (NH_4OH), sodium nitrate ($NaNO_3$), and sodium dihydrogen orthophosphate dihydrate ($NaH_2PO_4 \cdot 2H_2O$) were purchased from Merck and used without further purification. Barley straw was obtained from the Topflite Company in Christchurch, New Zealand.

Preparation of iron-treated barley straw biochar (Fe-BSBC)

The untreated barley straw was washed and dried in an oven at 60 °C for 24 h. Then, the dried samples were ground and sieved to a particle size of 0.6–1.18 mm. To prepare barley straw biochar (BSBC), the samples were pyrolyzed under oxygen-limited conditions at 600 **°C** for 2 h. This temperature was selected based on the findings of Sedmihradská et al. (2020), who identified 600 °C as the optimal temperature for producing biochar from barley straw, enhancing its stability and adsorption properties.

The Fe-BSBC composites were prepared using a method similar to that outlined in a previous study by Perera et al. (2024), which demonstrated excellent performance for phosphate removal. Still, its effectiveness for nitrate removal was not explored. Briefly, the prepared biochar was immersed in 1 M Fe (III) chloride dissolved in a saturated sodium chloride (NaCl) solution. The suspension was placed under a vacuum while stirring for up to 2 h. The iron (III) chloride solution was decanted, and the treated biochar was dried at 60 °C for 24 h. The treated material was then immersed in a 5 M ammonium hydroxide (NH_4OH) solution. The pH of the solution was adjusted to 9–10 while stirring, and then left for 3 h to allow the formation of iron (III) hydroxide. The suspension was left to settle overnight, and the treated biochar was then washed extensively with DI water until the pH of the wash water reached 7. The treated biochar sample was subsequently dried at 60 °C for 24 h.

Characterization of Fe-BSBC

Surface functional groups on Fe-BSBC were identified using Fourier transform infrared (FTIR) spectroscopy, covering a range of 400 to 4000 cm^{-1}, with a L1600300 Spectrum TWO LiTA system (UK). Scanning electron microscopy (SEM) with a JEOL JSM IT-300LV was employed to examine the surface morphology of the adsorbent. EDS analysis was conducted to investigate the elemental composition of Fe-BSBC before and after adsorption, using an Oxford X-Max 50 from Oxford Instruments. Crystallinity was assessed with a Rigaku Smartlab 3 kW X-ray diffractometer employing CuK(α) radiation. The zeta potential of the adsorbent was measured using a Zetasizer Nano (Malvern Panalytical) and analyzed with Zetasizer Software version 8.01.4906. The specific surface area of Fe-BSBC was determined by the Brunauer–Emmett–Teller (BET) multipoint method, while pore size distribution was analyzed using the Barrett-Joyner-Halenda (BJH) method, with an Autosorb iQ instrument from Anton Paar Ltd., Austria.

Effect of operational factors on adsorption (contact time, adsorbent dosage, adsorbate concentration, pH, competing anions)

Batch adsorption experiments were conducted by adding Fe-BSBC up to a final concentration of 5 g/L to 100 mL of a solution of either nitrate or phosphate with a concentration of 15 g/L in 120-mL plastic test tubes. The dosages were selected based on preliminary experiments, which showed that a high adsorbent dosage is required for effective nitrate removal compared to phosphate. The test tubes were placed in an orbital shaker at 220 rpm for 48 h to ensure equilibrium was reached, as indicated by the stabilized pollutant concentrations in the solution. Afterwards, the samples were filtered through 0.45-µm PTFE membrane filters, and the nitrate and phosphate concentrations were measured using a Dionex ICS-3000 Reagent-Free™ Ion Chromatography (RFIC™) system.

Various adsorption experiments were performed to investigate the impact of different adsorbent dosages, pH levels, and competing anions, along with kinetic and isotherm analyses. The experimental conditions are summarized in Table 1. All experiments were conducted in triplicate at a pH of 6 and a temperature of 23 ± 1 °C, with the mean values ± standard deviation reported. The pH of the solution was adjusted to 2–9 using NaOH and HCl to evaluate the impact of pH on adsorbent performance. The adsorption efficiency (R, %) and capacity (q_e, mg/g) of NO_3^- and PO_4^{3-} by Fe-BSBC were determined using Eqs. 1 and 2, respectively.

$$R(\%) = (C_0 - C_e)/C_0 \times 100 \quad (1)$$

$$q_e = (C_0 - C_e) \times V/m \quad (2)$$

where V (L) is the volume of the solution, C_0 and C_e (mg/L) are the initial and equilibrium concentrations of NO_3^- and PO_4^{3-}, respectively, and m is the Fe-BSBC mass.

Kinetic and isotherm model fitting

To investigate the mechanisms governing the adsorption process and identify the potential rate-limiting steps, two non-linear kinetic models, the pseudo-first-order (PFO) and pseudo-second-order (PSO) models, were applied to fit the

Table 1 Experimental parameters for adsorption experiments

Adsorption experiment	Initial concentration, mg/L	Fe-BSBC mass, g/100 mL	Sampling time, h	pH
Effect of contact time and kinetic study	NO_3^- or PO_4^{3-} = 15	NO_3^- = 1.5 PO_4^{3-} = 0.5	NO_3^-, $PO_4^{3-=}$ 0.02–48	6
Effect of adsorbate concentration and Isotherm study	NO_3^- or PO_4^{3-} = 15–250	NO_3^- = 1.5 PO_4^{3-} = 0.5	NO_3^- = 24 PO_4^{3-} = 8	6
Effect of solution pH	NO_3^- or PO_4^{3-} = 15	NO_3^- = 1.5 PO_4^{3-} = 0.5	NO_3^- = 24 PO_4^{3-} = 8	2–9
Effect of competing anions	NO_3^-, PO_4^{3-}, SO_4^{2-}, and Cl^- = 15	NO_3^- = 1.5 PO_4^{3-} = 0.5	NO_3^- = 24 PO_4^{3-} = 8	6
Effect of adsorbent dosage	NO_3^- or PO_4^{3-} = 15	NO_3^- = 0.1, 0.5, 1.0, 1.5, 2.0 PO_4^{3-} = 0.05, 0.1, 0.25, 0.5, 0.7	NO_3^- = 24 PO_4^{3-} = 8	6

experimental data. Meanwhile, three non-linear adsorption isotherm models, including Langmuir, Freundlich and Sips, were used to analyze the adsorption results of NO_3^- and PO_4^{3-} onto Fe-BSBC. These models are widely used in adsorption kinetics and isotherm studies (Ghaedi 2021). The experimental conditions for kinetic and isotherm studies are presented in Table 1. The equations for the kinetic and isotherm models are shown in Table 2.

Statistical analysis

All adsorption experiments were performed in triplicate, and results are reported as mean values ± standard deviation. The appropriateness of the kinetic and isotherm models in fitting the experimental data was evaluated using the coefficient of determination (R^2) and the mean squared error (MSE). A two-sample *t*-test ($p \leq 0.05$) was performed to statistically evaluate the effect of competing anions on the removal efficiency of nitrate and phosphate. Data analysis, including calculation of means, standard deviations, and non-linear regression, was carried out using Microsoft Excel version 2403.

Results and discussion

Impact of contact time

The identification of the contact time required for the adsorbent to reach equilibrium under a given condition is a critical part of adsorption studies. Figure 1 illustrates the impact of contact time on NO_3^- and PO_4^{3-} removal efficiency (R, %) and adsorption capacity (q, mg/g) using Fe-BSBC. As shown in Fig. 1, PO_4^{3-} removal occurred considerably faster than NO_3^- removal. Phosphate adsorption equilibrium was achieved within 8 h, with its removal efficiency rising rapidly from 59% at 10 min to a maximum of 98% at equilibrium. The PO_4^{3-} adsorption capacity also showed a rapid increase, stabilizing at 2.61 mg/g, almost three times that of NO_3^-. The quick attainment of equilibrium indicates that Fe-BSBC exhibits a high affinity for PO_4^{3-} ions. In contrast, NO_3^- removal was slower, reaching equilibrium after 24 h (Fig. 1). Nitrate removal efficiency increased from 6% at 10 min to a maximum of 81% at equilibrium time. The corresponding adsorption capacity rose steadily, stabilizing at 0.79 mg/g. The longer contact time required for NO_3^- adsorption to reach

Table 2 Kinetic and isotherm model equations

Models	Equations	Nomenclature
Kinetic		
Pseudo-first order (PFO)	$q_t = q_e(1 - \exp(-k_1 t))$	q_t (mg/g), adsorption capacity at time t; q_e (mg/g), adsorption capacity at equilibrium; k_1 (h^{-1}), PFO rate constant; k_2 (g/mg/h), PSO rate constant
Pseudo-second order (PSO)	$q_t = \frac{(k_2 q_e^2 t)}{1 + k_2 q_e t}$	
Isotherms		
Langmuir	$q_e = \frac{q_{max} K_L C_e}{1 + K_L C_e}$	q_e (mg/g), adsorption capacity at equilibrium; C_e (mg/L), NO_3^- and PO_4^{3-} concentration at equilibrium; K_L (L/mg), Langmuir isotherm constant; q_{max} (mg/g), maximum adsorption capacity; K_f, Freundlich isotherm constant; n (dimensionless), Freundlich exponent; bs (L/mg), affinity constant
Freundlich	$q_e = K_f C_e^{1/n}$	
Sips	$q_e = \frac{q_{max} b_s C_e^{1/n}}{1 + b_s C_e^{1/n}}$	

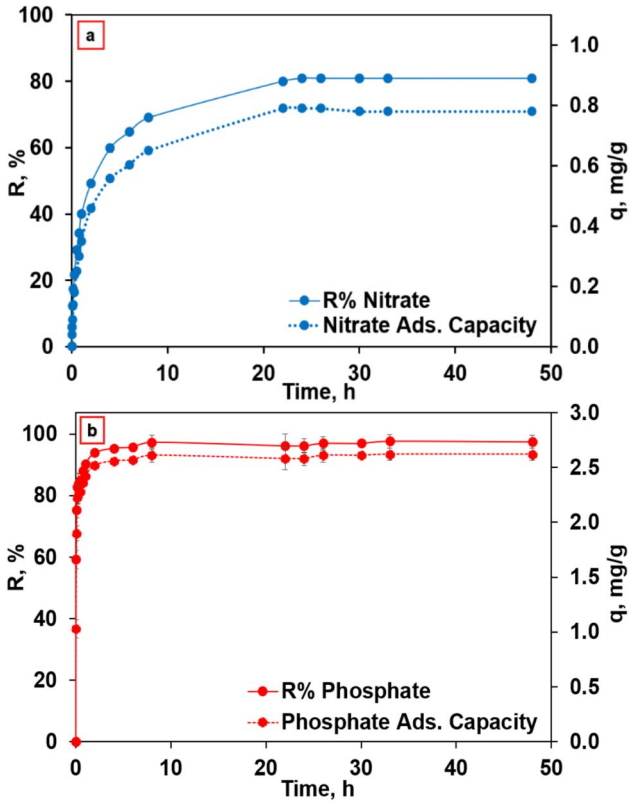

Fig. 1 Impact of contact time on removal efficiency (R%) and adsorption capacity (q) of (**a**) nitrate and (**b**) phosphate by Fe-BSBC

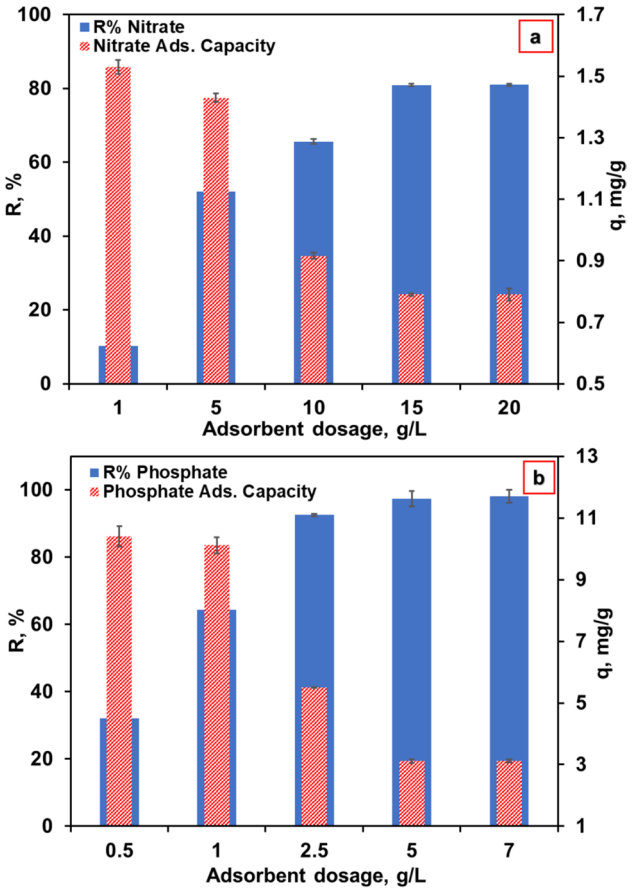

Fig. 2 Impact of adsorbent mass on (**a**) nitrate and (**b**) phosphate removal efficiency (R %) and adsorption capacity (q_e)

equilibrium could be attributed to weaker interactions between NO_3^- ions and the adsorbent or higher mass transfer resistance. These distinct adsorption kinetics underscore the importance of tailoring the contact time to the target contaminant to optimize treatment efficiency. In general, Fe-BSBC demonstrated excellent performance in removing both nitrate and phosphate, with phosphate removal being more effective. This difference is likely due to the multi-charged nature of PO_4^{3-} ions, which results in stronger electrostatic interactions with the positively charged active sites on Fe-BSBC (Baidas et al. 2023). Phosphate's ability to form complexes, along with the stronger binding affinity of iron (III) (Fe^{3+}) for phosphate anions compared to nitrate, results in stronger binding and higher phosphate removal (Min et al. 2020). A high porosity, a large specific surface area, and the presence of various functional groups have been demonstrated to be crucial for nitrate removal (Parker et al. 2012). However, the reduction in the biochar's surface area after iron treatment, as described later in the "Adsorbent characterization" section, could also contribute to its lower nitrate removal capacity compared to phosphate. Based on these results, equilibrium contact times of 8 h for PO_4^{3-} and 24 h for NO_3^- were established for subsequent adsorption experiments.

Impact of adsorbent mass

The relative percentage removal efficiency of both pollutants increased with the Fe-BSBC dosage, reaching a plateau at a dosage of 15 g/L for nitrate and 5 g/L for phosphate, with higher dosages yielding only a slight improvement in removal performance (Fig. 2). A significant improvement was observed in nitrate removal (from 10 to 81%) as the adsorbent mass increased from 1 to 20 g/L (Fig. 2a). The phosphate removal followed the same trend, with the removal efficiency improving from 32 to 98% as the adsorbent mass increased from 0.5 to 7 g/L (Fig. 2b). The observed increase in removal efficiency can be attributed to the greater number of cationic sorption sites available for ionic attraction, resulting from a higher concentration of Fe-BSBC. At the same time, the nitrate adsorption capacity decreased from 1.53 to 0.79 mg/g, and the phosphate adsorption capacity diminished from 9.90 to 2.63 mg/g as the adsorbent dosage increased, suggesting an excessive

number of sorption sites available. Therefore, dosages of 15 g/L for nitrate and 5 g/L for phosphate were selected for subsequent adsorption experiments. The lower dosage of Fe-BSBC required to effectively remove PO_4^{3-} compared to NO_3^- ions is related to the higher affinity of the adsorbent for phosphate, as discussed above.

Impact of pH

The Fe-BSBC exhibited high nitrate adsorption across a broad pH range of 2 to 8 (Fig. 3-left(a)). Nitrate removal remained at 80% or higher throughout this entire pH range. The highest removal efficiency, 86%, was observed at pH 2. As the pH increased, the removal efficiency slightly decreased, reaching 80% at pH 10. The adsorption capacity followed a similar trend, with the highest value of 0.85 mg/g at pH 2. Adsorption capacity gradually declined as the pH increased, stabilizing at 0.79 mg/g between pH 6 and pH 10. The results demonstrate that nitrate adsorption by Fe-BSBC is somewhat pH-dependent, with acidic conditions and a higher concentration of protons (H^+ cations) being the most favourable for nitrate removal. At lower pH values, increased protonation of the adsorbent surface functional groups enhances electrostatic interactions with negatively charged nitrate ions, resulting in higher adsorption performance (Haghighi Mood et al. 2024). At higher pH levels, reduced protonation and increased competition from hydroxide ions (OH^-) likely contribute to the slightly reduced nitrate removal efficiency (Khoshkalam et al. 2023). Furthermore, NO_3^- ions can also form hydrogen bonds with protonated surface hydroxyl groups on iron oxides (Dewage et al. 2018). A similar trend was reported by Dewage et al. (2018), Usman et al. (2016), and Haghighi Mood et al. (2024).

Figure 3-left(b) also shows that a high phosphate removal efficiency was maintained in the pH range of 2–6, with a maximum value of 98% observed at pH 6. A decline in removal efficiency occurred at higher pH levels, with values decreasing to 88% at pH 8 and 86% at pH 10. The adsorption capacity followed a similar trend, peaking at 2.61 mg/g at pH 6. At pH levels of 8 and 10, the adsorption capacity decreased to 2.37 mg/g and 2.33 mg/g, respectively. Optimal removal performance at lower pH values can be attributed

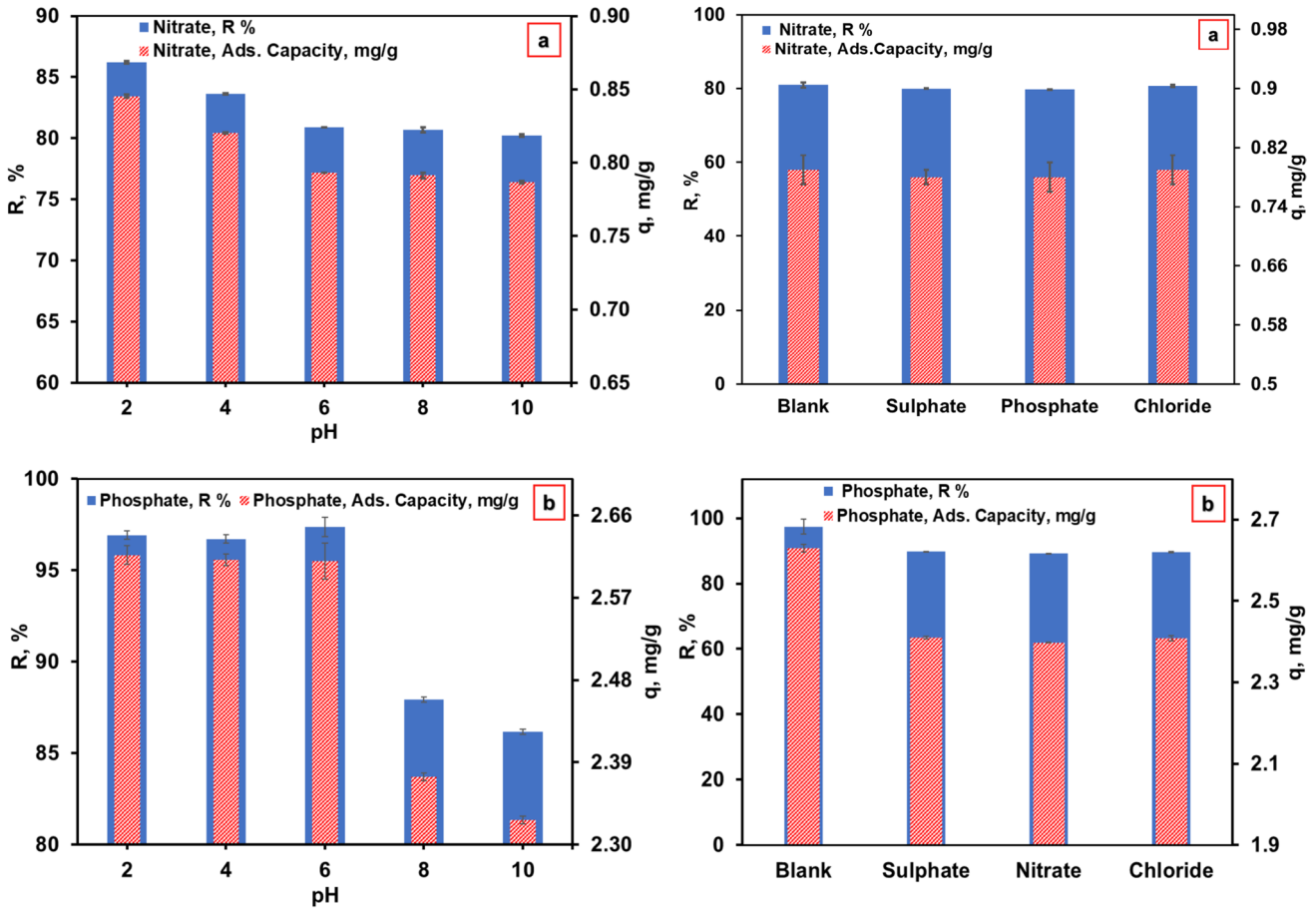

Fig. 3 Impact of pH (left column) and competing anions (right column) on removal efficiency (R%) and adsorption capacity (q_e) of (**a**) nitrate and (**b**) phosphate

to the increased positive charge on the adsorbent surface due to the higher availability of H^+ ions, which leads to electrostatic attraction between the active adsorption sites on the adsorbent and phosphate. At higher pH values, the concentration of hydroxide ions (OH^-), which compete with phosphate ions for sorption sites, increased (Wang et al. 2012). Additionally, at low pH values, $H_2PO_4^-$ is the dominant species and is more readily adsorbed on metal hydroxide adsorbents than HPO_4^{2-} due to the formation of hydrogen bonds between the adsorbent surface and one of its protons (Chubar et al. 2005). The efficient phosphate adsorption onto iron-modified biochar has been linked to the electrostatic attraction between the adsorbent's active sites and the $H_2PO_4^-$ species (Yang et al. 2018). A similar pattern was observed by Ou et al. (2023), Delgadillo-Velasco et al. (2021) and Wang et al. (2012), who used iron-modified carbon and iron-doped activated carbon for phosphate adsorption from water. Their findings indicated that phosphate removal is more effective in acidic conditions and declines at alkaline pH levels (pH > 7).

Impact of competing anions

Typical anions commonly found in groundwater and natural water, such as chloride and sulphate, compete with nitrate and phosphate ions for the adsorbent's cationic sites (Banu et al. 2019). The competing effect of these ions was examined by adding 1.5 g and 0.5 g of the Fe-BSBC composite for nitrate and phosphate uptake, respectively, to 100 mL of a 15 mg/L solution containing the competing ion mixed with the corresponding adsorbate anions (with a blank control with no competing ions). The results, illustrating the influence of these ions on nitrate and phosphate uptake, are shown in Fig. 3-right. They indicate that sulphate, phosphate, and chloride ions have minimal impact on nitrate removal by Fe-BSBC (Fig. 3-right(a)). A paired two-sample *t*-test ($p \leq 0.05$) was conducted to assess performance variations, confirming no significant difference in nitrate removal in the presence of competing anions ($p > 0.05$). This demonstrates the material's selectivity for nitrate over other common anions in water, making it a promising adsorbent for nitrate removal in polluted waters typically containing competing ions. However, the presence of sulphate, nitrate, and chloride ions interfered with phosphate removal by Fe-BSBC (Fig. 3-right(b)), with a *p*-value < 0.05. Despite this, the material retains relatively high phosphate removal efficiency (above 89%), demonstrating its potential for phosphate removal in water containing multiple competing anions. Nevertheless, the different impact of competing cations on phosphate and nitrate adsorption could be the result of differences in the molarity of the test solutions, in which nitrate molarity was the highest, meaning more NO_3^- ions were available to adsorb onto Fe-BSBC.

Adsorption kinetic models

Figure 4-left shows the kinetic profiles of nitrate and phosphate removal by Fe-BSBC, modelled using PFO and PSO equations. The experimental data for both nitrate and phosphate more closely follow the PSO model, both during the initial rapid adsorption phase and in the subsequent equilibrium, as evidenced by the higher R^2 values. Table 3 presents the kinetic model parameters for nitrate and phosphate adsorption. The PSO model has a higher R^2 value (0.9893) compared to the PFO model (0.9619) for nitrate, indicating a slightly better fit. Phosphate adsorption is much better described by the PSO model, with an R^2 value of 0.9799 compared to 0.8983 for the PFO model. Furthermore, the similarity between the calculated and experimental q_e values suggests that the PSO model effectively describes the adsorption of both nitrate and phosphate onto Fe-BSBC. This suggests that chemisorption likely governs the adsorption mechanism of Fe-BSBC. This is consistent with the studies of Kuang et al. (2023), Delgadillo-Velasco et al. (2021), Usman et al. (2016), and Wang et al. (2012). The first two studies focused on the use of iron-modified reed waste biochar and iron-modified *Conocarpus* biochar for nitrate removal from aqueous solutions, respectively, while the latter two examined iron-modified carbon and iron-doped activated carbon for phosphate adsorption.

Adsorption isotherm models

Nitrate and phosphate concentrations ranging from 15 to 250 mg/L were used to generate isotherm data. As shown in Fig. 4-right, while the nitrate and phosphate concentration increased from 15 to 250 mg/L, the experimental nitrate adsorption capacity rose from 0.79 to 2.04, and for phosphate increased from 2.61 to 13.73, suggesting the presence of numerous unsaturated adsorption sites. The Langmuir, Freundlich, and Sips models were fitted to experimental adsorption data (Fig. 4-right). The experimental data align well with the Freundlich and Sips isotherm model for both adsorbates, particularly at higher concentrations. Table 4 summarizes the parameters of the isotherm models. For both nitrate and phosphate adsorption, the Freundlich and Sips models exhibit the highest R^2 values (close to 1), suggesting that the adsorption data fit these models well. These results suggest that Fe-BSBC has a strong affinity for both nitrate and phosphate, with adsorption occurring predominantly through a heterogeneous mechanism.

Table 5 shows a comparative analysis of nitrate and phosphate adsorption capacities among various iron-modified adsorbents. The maximum adsorption capacities of Fe-BSBC derived from the Sips model for nitrate and phosphate in the studies reported here were found to be 4.07 mg/g and 22.0 mg/g, respectively. However, the highest

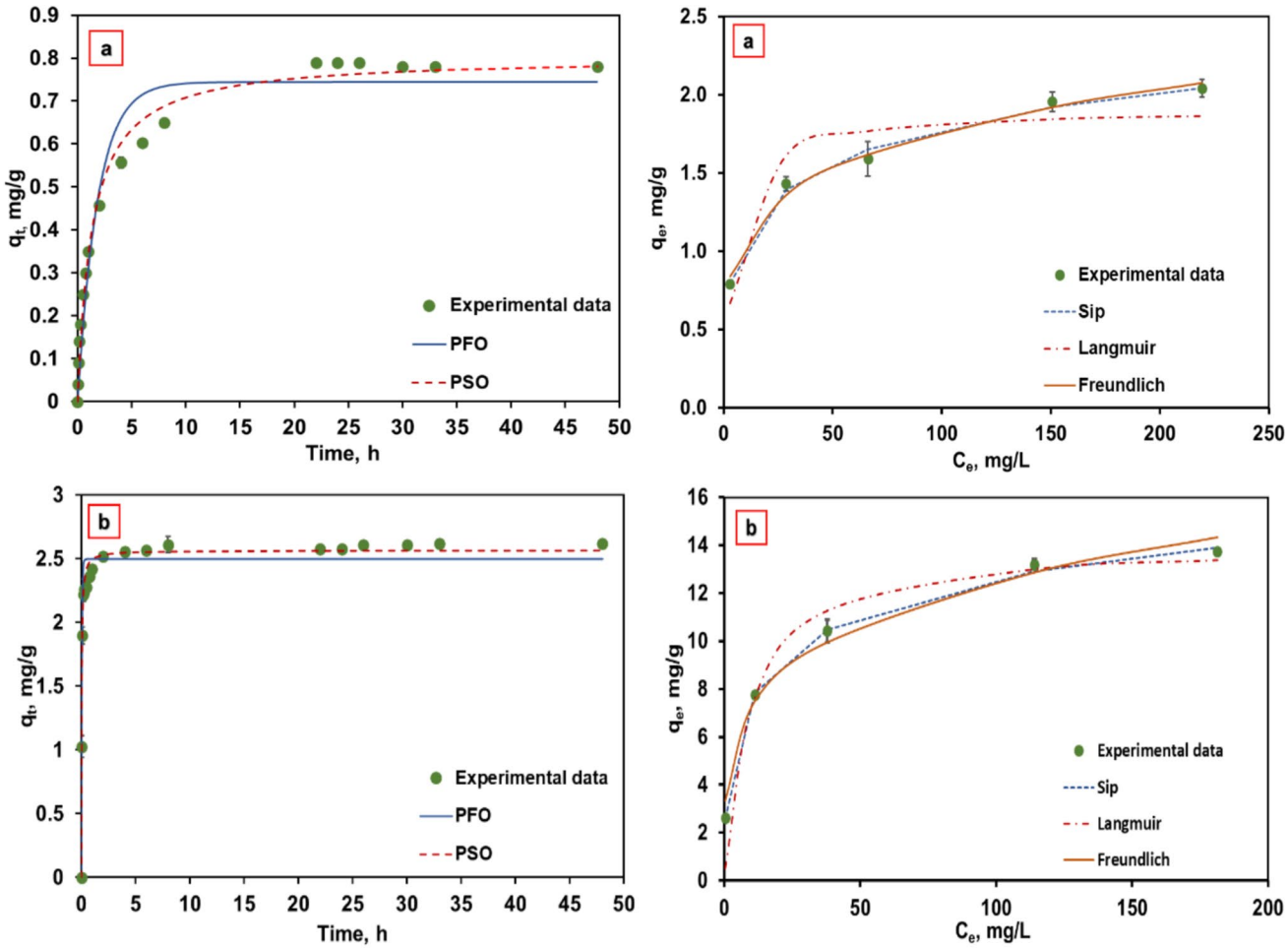

Fig. 4 Adsorption kinetics (left column) and isotherms (right column) for (**a**) nitrate and (**b**) phosphate removal using Fe-BSBC

adsorption capacities experimentally measured were about half of the theoretical values predicted by the Sips model, i.e. 2.0 mg/g for nitrate and 13.7 mg/g for phosphate. Still, the Fe-BSBC's adsorption capacity compares well to other adsorbents. For instance, iron-modified *Conocarpu* biochar exhibited a nitrate adsorption capacity of only 1.924 mg/g (Usman et al. 2016), and iron-functionalized commercial

Table 3 Parameters of kinetic models for nitrate and phosphate adsorption by Fe-BSBC

Model	Parameters	NO_3^-	PO_4^{3-}
Pseudo-first-order (PFO)	k_1 (h^{-1})	0.541	23.58
	q_e (mg/g)	0.745	2.42
	R^2	0.9619	0.8983
	MSE	0.004	0.022
Pseudo-second-order (PSO)	k_2 (g/mg h^{-1})	0.936	15.19
	q_e (mg/g)	0.803	2.53
	R^2	0.9893	0.9799
	MSE	0.001	0.004

Table 4 Parameters of isotherm models for nitrate and phosphate adsorption by Fe-BSBC

Model	Parameter	NO_3^-	PO_4^{3-}
Langmuir	$q_{max,}$ mg/g	1.91	14.06
	K_L, L/mg	0.19	0.11
	R^2	0.8816	0.9784
	MSE	0.025	1.07
Freundlich	K_f, (mg/g) $(L/mg)^{1/n}$	0.68	4.26
	n	4.82	4.29
	R^2	0.9893	0.9856
	MSE	0.002	0.259
Sips	$q_{max,}$ mg/g	4.07	22
	$b_{s,}$ L/mg	0.17	0.21
	n	3.07	2.43
	R^2	0.993	0.9986
	MSE	0.001	0.023

Table 5 Comparison of nitrate and phosphate uptake capacities among various iron-modified adsorbents

Adsorbent	Adsorbate	Maximum adsorption capacity, mg/g	Reference
Iron-functionalized pine woodchips (Fe-WC)	PO_4^{3-}	8.17	Perera et al. 2024
Iron-functionalized commercial biochar (Fe- PyOM)		6.27	
Iron/calcium oxide-modified bamboo biochar (ZFCO-BC)		58.24	Ou et al. 2023
Iron-doped activated carbon		8.73	Wang et al. 2012
Iron-modified carbon		23.33	Delgadillo-Velasco et al. 2021
Iron-loaded Okara		16.39	Nguyen et al. 2014
$FeCl_3$-modified waste Douglas fir biochar	NO_3^-	20.67	Haghighi Mood et al. 2024
$FeCl_3$-Modified Reed Waste Biochar		272.024	Kuang et al. 2023
$FeCl_3$- modified corncob biochar		32.33	Long et al. 2019
α-Fe_2O_3/Fe_3O_4 waste Douglas fir biochar		15	Dewage et al. 2018
Iron-modified conocarpu biochar		1.924	Usman et al. 2016
Fe-BSBC	NO_3^-	4.07	This study
	PO_4^{3-}	22	

biochar (Fe-PyOM) had a phosphate adsorption capacity of 6.27 mg/g. Similarly, iron-functionalized pine woodchips (Fe-WC) showed a phosphate adsorption capacity of 8.17 mg/g (Perera et al. 2024). Although some other studies, such as those by Kuang et al. (2023) and Long et al. (2019), report higher nitrate adsorption capacities of 272 mg/g and 32.3 mg/g, respectively, Fe-BSBC remains a promising candidate, particularly for phosphate removal. Fe-BSBC phosphate adsorption capacity of 13.7 mg/g is particularly notable, surpassing that of several other iron-modified adsorbents listed in Table 5. These findings demonstrate that Fe-BSBC is a viable and competitive option for nitrate and phosphate removal, making it a promising candidate for environmental remediation applications.

Adsorbent characterization

The Fe-BSBC exhibited a BET surface area of 221.6 m^2/g, which was lower than the 372.7 m^2/g observed for BSBC without Fe-activation, likely due to the presence of iron oxides (FeO_x), which generally possess relatively low surface areas and may block some of the pores of the biochar (Chen et al. 2011). However, the average pore diameter of Fe-BSBC (4.055 nm) was slightly larger than that of BSBC (3.858 nm), suggesting the presence of a mesoporous structure. Similarly, the pore volume of Fe-BSBC (0.081 cm^3/g) exceeded that of BSBC (0.011 cm^3/g).

The morphological properties and microstructure of the BSBC and Fe-BSBC were examined using SEM analysis. As shown in Fig. 5a, BSBC exhibited an aggregated and

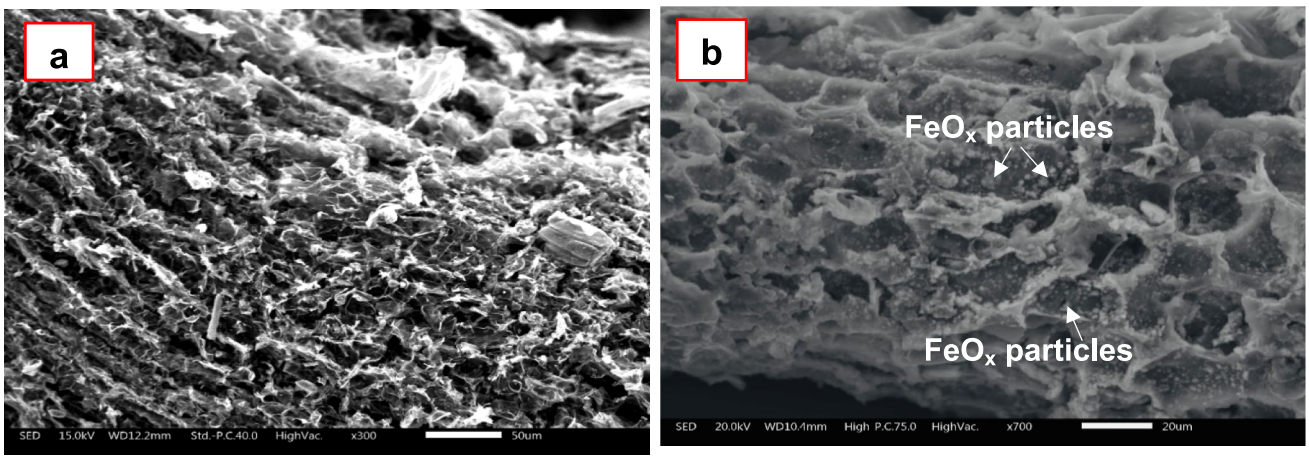

Fig. 5 SEM image of (**a**) BSBC, and (**b**) Fe-BSBC

interconnected structure, with noticeable roughness and porosity. The SEM images of Fe-BSBC (Fig. 5b) confirmed the successful incorporation of Fe onto both the surface and within the pore structure of the biochar. Figure 5b clearly shows that fine and aggregated particles are uniformly distributed across the surface of Fe-BSBC. These particles exhibit some clustered aggregation, which is possibly due to the formation of FeO_x crystal on the biochar surface, confirming that the surface of the functionalized media was coated with iron hydroxide deposits (Perera et al. 2024). Furthermore, while some of the pore structure of the biochar is obstructed by iron, a thin iron oxide layer forms on the biochar surface, enhancing the adsorption and immobilization of anions (Min et al. 2020). These findings align with previous studies on iron-modified biochar, indicating that iron oxide particles can integrate with the carbon matrix during the iron functionalization process (Kuang et al. 2023; Usman et al. 2016).

The EDS spectra provide insights into the elemental composition of Fe-BSBC before and after pollutant adsorption, revealing changes in surface chemistry due to adsorption processes. Figure 6 shows that carbon (C) is the main element in the biochar structure, as expected with a cellulosic material. A substantial increase in iron content (Fe: 36%) was observed after Fe treatment, confirming successful iron functionalization. Although EDS signals for N and P were not clearly detected, possibly due to their low concentrations or distribution across the surface in non-crystalline forms, indirect evidence suggests their adsorption. After nitrate adsorption (Fe-BSBC-N) (Fig. 6), the iron content decreased, which may suggest partial surface coverage of Fe sites by nitrate ions or changes in the local environment around Fe atoms, reducing their EDS signal. A further decrease in Fe signal after phosphate adsorption (Fe-BSBC-P) (to 6.8 wt%) supports the formation of Fe–O–P complexes through ligand exchange, where phosphate likely displaced hydroxyl groups on Fe $(OH)_3$. An increase in relative oxygen content after nitrate adsorption and the high oxygen content remaining after phosphate adsorption suggest surface interactions with Fe$(OH)_3$ sites.

The role of electrostatic attraction in nitrate and phosphate adsorption was further confirmed by zeta potential analysis. Fe-BSBC initially exhibited a zeta potential of 0.584 ± 0.22 mV, indicating a near-neutral to slightly positive surface charge due to the presence of iron hydroxides. After nitrate adsorption, the zeta potential dropped to -0.1 ± 0.02 mV, suggesting the attachment of negatively charged NO_3^- ions through electrostatic interactions. Following phosphate adsorption, the zeta potential decreased further to -0.2 ± 0.01 mV, reflecting the stronger binding

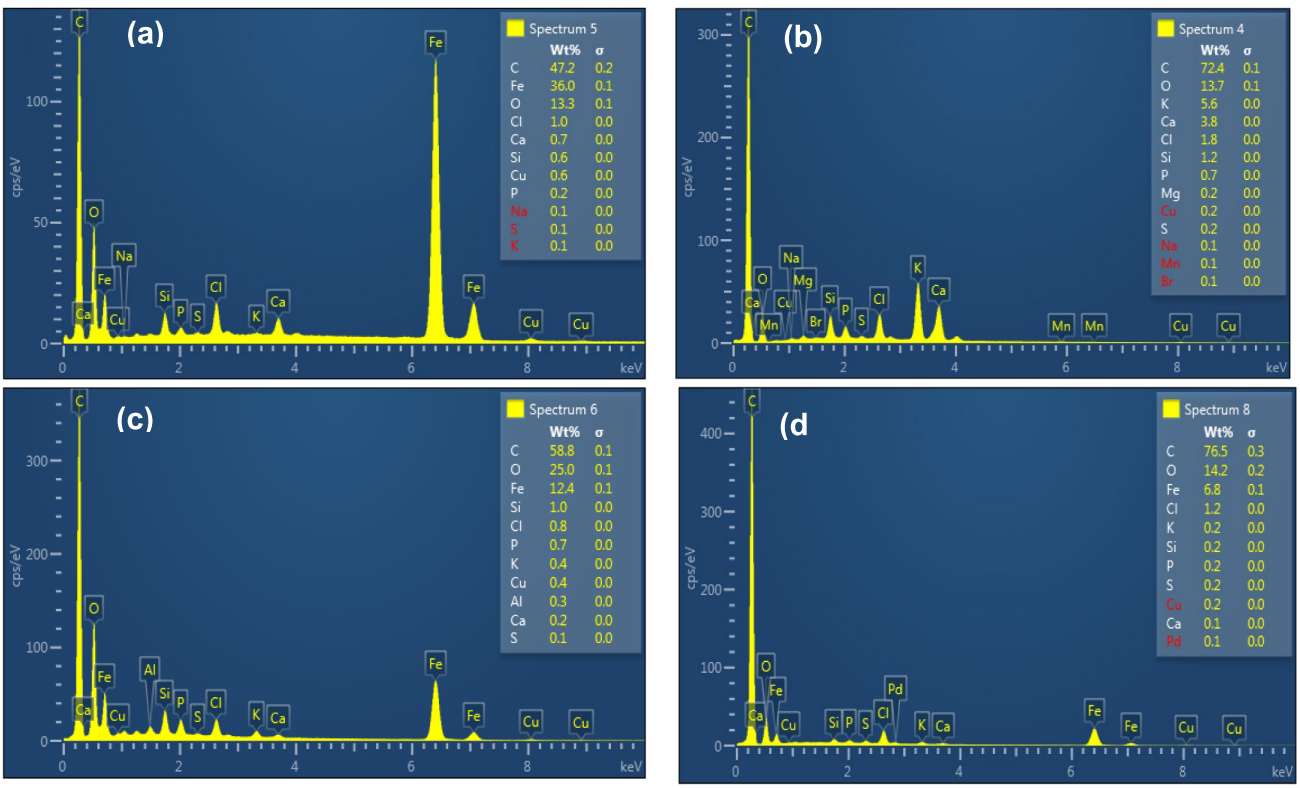

Fig. 6 EDS image of (**a**) BSBC, (**b**) Fe-BSBC, (**c**) Fe-BSBC-N, and (**d**) Fe-BSBC-P

of highly negatively charged PO_4^{3-} ions. This likely happens through both electrostatic attraction and inner-sphere complexation with Fe-OH groups via ligand exchange.

Fe-BSBC exhibited various functional groups before and after adsorption of nitrate and phosphate, as illustrated in Fig. 7(a). Both the pristine and post-adsorption Fe-BSBC samples (after nitrate (Fe-BSBC-N) and phosphate (Fe-BSBC-P) removal) exhibited a broad O–H peak at around 3660 cm^{-1}, suggesting the existence of hydroxyl groups on the surface (Kuang et al. 2023; Perera et al. 2018). The peak at 2932 cm^{-1} corresponds to C–H stretching of aliphatic groups (methyl and methylene) commonly found in organic compounds (Ramírez-Montoya et al. 2014; Wang et al. 2016). The peak at 1687 cm^{-1} is attributable to the O–H deformation and bending vibrations in Fe-BSBC (Fu and Quan 2006). The peak at 1106 cm^{-1} is indicative of various stretching vibrations of C-O and O-C-O (Vaughn et al. 2017). The aromatic C-H bending was identified by the band at 834 cm^{-1}, which suggests the presence of aromatic rings (Guo et al. 2017). The peak around 1076 cm^{-1} could be attributed to C–OH groups (Lu and Oza 2013). The peaks observed at 439.05 cm^{-1} and 618 cm^{-1} were identified as Fe–O adsorption peaks, suggesting that iron was successfully incorporated into the biochar (Xie et al. 2014).

The appearance of the 1379 cm^{-1} peak after nitrate adsorption corresponds to N–O stretching vibrations, confirming the adsorption of nitrate ions onto Fe-BSBC (Sembiring et al. 2014; Choe et al. 2010). The bands at 666 cm^{-1} and 424.5 cm^{-1} may be associated with changes in Fe-related vibrations due to interaction with nitrate ions. After phosphate adsorption, the peak at 1018 cm^{-1} was identified as covalent-like Fe–O–P bonds (Xie et al. 2014), indicating the formation of iron-phosphate complexes upon phosphate adsorption. The shift in Fe-related peaks (671 cm^{-1} and 423 cm^{-1}) suggests structural modifications due to phosphate binding.

The diffraction patterns of the Fe-BSBC before and after nitrate and phosphorus adsorption were examined using XRD, as illustrated in Fig. 7(b). Clearly, the Fe-BSBC has a mainly amorphous structure, as indicated by the XRD patterns, which do not exhibit sharp peaks. A broad peak between 20° and 25° is observed, which corresponds to amorphous carbon and modified cellulose structures (Perera et al. 2024; Min et al. 2020; Zheng et al. 2020). The peak at 36° is associated with Fe–O bonds, confirming the presence of iron hydroxide or iron oxide species (Mohan et al. 2014), which was confirmed by the peaks of 439.05 cm^{-1} and 618 cm^{-1} in FTIR spectra (Fig. 7(a)). The peak at 47° further supports the presence of iron hydroxide ($Fe(OH)_3$).

The peak at 44° emerges after nitrate adsorption, suggesting a structural rearrangement of iron species, possibly indicating the partial transformation of $Fe(OH)_3$ to Fe_3O_4 (magnetite) (Perera et al. 2024). The XRD results indicate that NO_3^- adsorption does not cause significant changes in peak locations, implying that the structure of Fe-BSBC remains largely unaffected (Fig. 7). This finding also suggests that electrostatic attraction is the primary mechanism behind NO_3^- adsorption (Haghighi Mood et al. 2024). Following phosphorus adsorption, a new peak observed at 57° confirmed the formation of $Fe_5(PO_4)_4(OH)_3$ (Liu et al. 2015) and phosphate complexation with iron hydroxide. The appearance of the 44° peak (which was not present before adsorption) suggests a structural modification of iron phases, potentially forming magnetite-like structures or Fe–O–P complexes, as confirmed by the peak at 1018 cm^{-1} in the FTIR analysis.

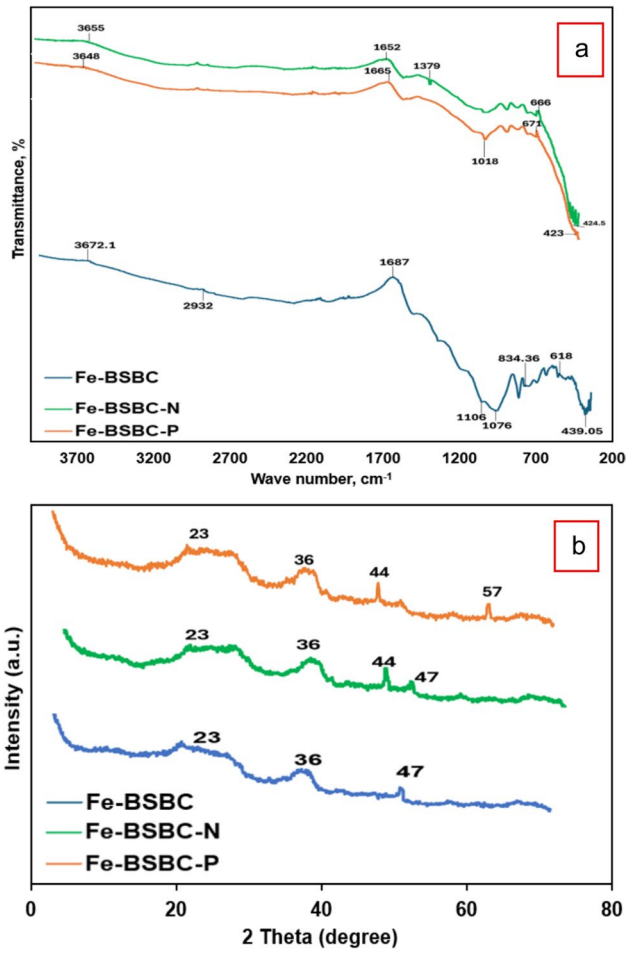

Fig. 7 Fe-BSBC adsorbent characterisation using (**a**) FTIR, and (**b**) XRD

Possible adsorption mechanisms of nitrate and phosphate by Fe-BSBC

Results from this study suggest that the adsorption of nitrate and phosphate onto Fe-BSBC is primarily governed by electrostatic interaction and surface complexation. The

solution pH plays a critical role in the electrostatic interaction between the adsorbent's surfaces and the adsorbate and, consequently, on adsorption performance. Nguyen et al. (2019) reported a point of zero charge (pH_{pzc}) of 6.88 for iron-modified biochar derived from rice straw. It would be expected that pH values lower than the pH_{pzc} would promote positively charged surfaces which favor anionic adsorption. This was observed in this study since the adsorption of nitrate and phosphate was the highest at pH 2 and 2–6, respectively, indicating that nitrate and phosphate can effectively interact with the positively charged sites on the Fe-BSBC at a solution pH of 2–6. At lower pH levels, the protonation of iron hydroxide functional groups on the Fe-BSBC enhances the positively charged surface, leading to the formation of $Fe–O^{+}H_2$ sites that electrostatically attract anions (Dewage et al. 2018). The decline is adsorption capacity at higher pH levels (pH 8–10) was more notorious for phosphate. Phosphate can be found predominantly as dihydrogen phosphate ($H_2PO_4^-$) at low pH (pH 3–7), and as hydrogen phosphate (HPO_4^{2-}) at higher pH levels (pH 7–12.5). At lower pH, a high positive surface charge on the Fe-BSBC favors the adsorption of $H_2PO_4^-$. As the pH increases above the pH_{pzc}, the Fe-BSBC surface tends to be negatively changed. Simultaneously, the dominant P species shifts to HPO_4^{2-} increasing the anionic charge. This results in a decline in electrostatic attraction and in phosphate adsorption capacity. Electrostatic interactions were further supported by zeta potential measurements. As previously described, Fe-BSBC exhibited a slightly positive surface charge, as indicated by zeta potential analysis. Upon nitrate and phosphate adsorption, the zeta potential shifted toward negative values, confirming the role of electrostatic attraction in the adsorption process.

Phosphate was more effectively adsorbed than nitrate, which could be explained by surface complexation as an additional adsorption mechanism. Kinetic analyses support the view of chemisorption as a dominant adsorption mechanism. Additionally, FTIR and XRD analyses provide direct evidence of Fe–O–P complex formation after phosphate adsorption, confirming the ligand exchange mechanism between phosphate and hydroxyl groups on iron hydroxide surfaces. The chemisorption of phosphate to iron oxides between pH 3–6 has been reported to occur through ligand exchange (Perera et al. 2024), whereby deprotonation of the iron hydroxyl group creates a reactive Fe site compatible with the oxygen in phosphate, creating different types of Fe–O coordination bonds, such as monodentate or bidentate complexes. This strong interaction differentiates phosphate adsorption from nitrate adsorption, as phosphate removal involves inner-sphere complexation via ligand exchange, whereas electrostatic attractions primarily drive nitrate adsorption. These findings highlight the dual adsorption mechanisms governing nitrate and phosphate removal and underscore phosphate's enhanced affinity due to inner-sphere complexation, a mechanism absent in nitrate adsorption.

Conclusions

This study demonstrates the potential of iron-modified biochar (Fe-BSBC), derived from locally sourced barley straw by-product and pyrolyzed at 600 °C for 2 h, as an effective adsorbent for nitrate and phosphate removal from water. The use of barley straw as a biochar precursor presents an environmentally sustainable and economically viable approach to nutrient removal in polluted water. Fe-BSBC exhibited an adsorption capacity of 13.7 mg/g for phosphate and 2.0 mg/g for nitrate, which is attributed to the formation of an iron oxide layer and a well-structured porous network. The adsorption process followed a pseudo-second-order kinetic model, indicating a chemisorption mechanism, while the Sips isotherm model suggested heterogeneous adsorption behavior. The primary adsorption mechanisms included electrostatic interactions, ligand exchange, and surface complexation, with phosphate removal being more strongly influenced by inner-sphere complexation. Phosphate removal experienced a slight decline due to interference from other anions, which was not observed in the adsorption of nitrate in the presence of competing anions. The findings of this study support the development of low-cost adsorption technologies for water treatment, particularly benefiting regions with limited access to advanced treatment technologies. Furthermore, the utilization of agricultural waste (barley straw) aligns with circular economy principles, reducing environmental pollution from stubble burning. There is also potential for using iron-treated biochar as an adsorbent for removing phosphate from agricultural runoff and nitrate from drinking water. To further optimize its practical application, future studies should focus on column experiments and desorption tests to assess the long-term performance and regeneration potential of Fe-BSBC.

Acknowledgements The authors gratefully acknowledge the laboratory technical support provided by Aude Thierry and Moeen Gholami from the Department of Civil & Environmental Engineering, Shaun Mucalo from the Department of Mechanical Engineering, Soongseok Yoon from the Department of Chemical and Process Engineering, and Matthew Polson from the School of Physical and Chemical Sciences at the University of Canterbury, Christchurch, New Zealand. Special thanks are also extended to Sumaira Basharat, PhD student, and Prof David Barker from the School of Chemical Sciences, Faculty of Science, University of Auckland, Auckland, New Zealand, for assisting with the FTIR analysis.

Author contribution Sepideh Ansari: Writing—original draft, Writing—review & editing, Data curation, Investigation, Visualization, Methodology, Formal analysis. Ricardo Bello-Mendoza: Writing—review & editing, Supervision, Validation, Methodology, Formal analysis. Aisling O'Sullivan: Writing—review & editing, Funding

acquisition, Supervision. All authors commented on previous versions of the manuscript. All authors read and approved the final manuscript.

Funding Open Access funding enabled and organized by CAUL and its Member Institutions. This work was supported by the Science for Technological Innovation (SfTI) National Science Challenges (NSC) Spearhead 9—Clean Water Technology (CWT) project (contract No. 2020-S9-CRS).

Data availability Data available from authors upon request.

Declarations

Ethical approval This is not applicable.

Consent to participate This is not applicable.

Consent for publication This is not applicable.

Competing interests The authors declare no competing interests.

References

Ahmed MJ, Hameed BH (2018) Adsorption behavior of salicylic acid on biochar as derived from the thermal pyrolysis of barley straws. J Clean Prod 195:1162–1169. https://doi.org/10.1016/j.jclepro.2018.05.257

Ahmed MJ, Anastopoulos I, Kalderis D, Danish M (2024) A comprehensive review of barley crop-based materials as adsorbents for the removal of aquatic pollutants. J Mol Liq. https://doi.org/10.1016/j.molliq.2024.125151

Anastopoulos I, Bhatnagar A, Hameed BH, Ok YS, Omirou M (2017) A review on waste-derived adsorbents from sugar industry for pollutant removal in water and wastewater. J Mol Liq 240:179–188. https://doi.org/10.1016/j.molliq.2017.05.063

Baidas S, Al-Deyain K, Meng X, Gao B (2023) Competitive removal of perchlorate ions by quaternary amine modified reed in the presence of nitrate and phosphate. Adsorpt Sci Technol. https://doi.org/10.1155/2023/3087629

Banu HT, Karthikeyan P, Meenakshi S (2019) Zr4+ ions embedded chitosan-soya bean husk activated bio-char composite beads for the recovery of nitrate and phosphate ions from aqueous solution. Int J Biol Macromol 130:573–583. https://doi.org/10.1016/j.ijbiomac.2019.02.100

Cai G, Ye ZL (2022) Concentration-dependent adsorption behaviors and mechanisms for ammonium and phosphate removal by optimized Mg-impregnated biochar. J Clean Prod 349:131453. https://doi.org/10.1016/j.jclepro.2022.131453

Chen B, Chen Z, Lv S (2011) A novel magnetic biochar efficiently sorbs organic pollutants and phosphate. Bioresour Technol 102(2):716–723. https://doi.org/10.1016/j.biortech.2010.08.067

Choe E, van der Meer F, Rossiter D, van der Salm C, Kim KW (2010) An alternate method for fourier transform infrared (ftir) spectroscopic determination of soil nitrate using derivative analysis and sample treatments. Water Air Soil Pollut 206(1–4):129–137. https://doi.org/10.1007/s11270-009-0091-z

Chubar NI, Kanibolotskyy VA, Strelko VV, Gallios GG, Samanidou VF, Shaposhnikova TO, Milgrandt VG, Zhuravlev IZ (2005) Adsorption of phosphate ions on novel inorganic ion exchangers. Colloids Surf A Physicochem Eng Asp 255(1–3):55–63. https://doi.org/10.1016/j.colsurfa.2004.12.015

Delgadillo-Velasco L, Hernández-Montoya V, Ramírez-Montoya LA, Montes-Morán MA, del Rosario Moreno-Virgen M, Rangel-Vázquez NA (2021) Removal of phosphate and aluminum from water in single and binary systems using iron-modified carbons. J Mol Liq 323:114586. https://doi.org/10.1016/j.molliq.2020.114586

Deng Y, Li M, Zhang Z, Liu Q, Jiang K, Tian J, Ni F (2021) Comparative study on characteristics and mechanism of phosphate adsorption on Mg/Al modified biochar. J Environ Chem Eng 9(2):105079. https://doi.org/10.1016/j.jece.2021.105079

Dewage NB, Liyanage AS, Pittman CU Jr, Mohan D, Mlsna T (2018) Fast nitrate and fluoride adsorption and magnetic separation from water on α-Fe2O3 and Fe3O4 dispersed on Douglas fir biochar. Bioresour Technol 263:258–265. https://doi.org/10.1016/j.biortech.2018.05.001

FAO (2023) Production: Crops and livestock products. In: FAOSTAT. Rome. https://www.fao.org/faostat/en/#data/QCL

Farouk SM, Mostafa NA, Abdelhamid S, Monazie AM (2021) Evaluation of utilizing sulfonated barely straw and coconut shell bio-adsorbents in removal of methylene blue dye from aqueous solutions. Port-Said Eng Res J 25(2):187–192. https://doi.org/10.21608/pserj.2021.67521.1100

Fu H, Quan X (2006) Complexes of fulvic acid on the surface of hematite goethite and akaganeite: FTIR observation. Chemosphere 63(3):403–410. https://doi.org/10.1016/j.chemosphere.2005.08.054

Garcia-Garcia G, Rahimifard S (2019) Life-cycle environmental impacts of barley straw valorisation. Resour Conserv Recycling 149:1–11. https://doi.org/10.1016/j.resconrec.2019.05.026

Ghaedi M (Ed.) (2021) Adsorption: fundamental processes and applications (vol 33). Academic Press, Amsterdam

Ghasemi SM, Ghaderpoori M, Moradi M, Taghavi M, Karimyan K (2020) Application of Box-Behnken design for optimization of malachite green removal from aqueous solutions by modified barley straw. Global NEST J. 22 (3) (2020) 390–399. https://journal.gnest.org/sites/default/files/Submissions/gnest_03089/gnest_03089_published.pdf

Guo W, Huo S, Feng J, Lu X (2017) Adsorption of perfluorooctane sulfonate (PFOS) on corn straw-derived biochar prepared at different pyrolytic temperatures. J Taiwan Inst Chem Eng 78:265–271. https://doi.org/10.1016/j.jtice.2017.06.013

Haghighi Mood S, Pelaez-Samaniego MR, Han Y, Mainali K, Garcia-Perez M (2024) Iron-and nitrogen-modified biochar for nitrate adsorption from aqueous solution. Sustainability 16(13):5733. https://doi.org/10.3390/su16135733

Hashemi F, Olesen JE, Dalgaard T, Børgesen CD (2016) Review of scenario analyses to reduce agricultural nitrogen and phosphorus loading to the aquatic environment. Sci Total Environ 573:608–626. https://doi.org/10.1016/j.scitotenv.2016.08.141

Ibrahim S, Wang S, Ang HM (2010) Removal of emulsified oil from oily wastewater using agricultural waste barley straw. Biochem Eng J 49(1):78–83. https://doi.org/10.1016/j.bej.2009.11.013

Inyang M, Gao B, Pullammanappallil P, Ding W, Zimmerman AR (2010) Biochar from anaerobically digested sugarcane bagasse. Bioresour Technol 101(22):8868–8872. https://doi.org/10.1016/j.biortech.2010.06.088

Inyang MI, Gao B, Yao Y, Xue Y, Zimmerman A, Mosa A, Cao X (2016) A review of biochar as a low-cost adsorbent for aqueous

heavy metal removal. Crit Rev Environ Sci Technol 46(4):406–433. https://doi.org/10.1080/10643389.2015.1096880
Jazini R, Soleimani M, Mirghaffari N (2018) Characterization of barley straw biochar produced in various temperatures and its effect on lead and cadmium removal from aqueous solutions. Water Environ J 32(1):125–133. https://doi.org/10.1111/wej.12307
Jones SE, Ding Y, Sabatini DA, Butler EC (2023) Nitrate uptake by cellulose-based anion exchange polymers derived from wheat straw. Water 15(20):3594. https://doi.org/10.3390/w15203594
Khoshkalam E, Fotovat A, Halajnia A, Kazemian H, Eshghi H (2023) Nitrate adsorption using green iron oxide nanoparticles synthesized by Eucalyptus leaf extracts: kinetics and effects of pH, KCl salt, and anions competition. J Mol Liq 375:121366. https://doi.org/10.1016/j.molliq.2023.121366
Kuang P, Cui Y, Zhang Z, Ma K, Zhang W, Zhao K, Zhang X (2023) Increasing surface functionalities of FeCl3-modified reed waste biochar for enhanced nitrate adsorption property. Processes 11(6):1740. https://doi.org/10.3390/pr11061740
Liu F, Zuo J, Chi T, Wang P, Yang B (2015) Removing phosphorus from aqueous solutions by using iron-modified corn straw biochar. Front Environ Sci Eng 9(6):1066–1075. https://doi.org/10.1007/s11783-015-0769-y
Liu R, Chi L, Wang X, Sui Y, Wang Y, Arandiyan H (2018) Review of metal (hydr) oxide and other adsorptive materials for phosphate removal from water. J Environ Chem Eng 6(4):5269–5286. https://doi.org/10.1016/j.jece.2018.08.008
Long L, Xue Y, Hu X, Zhu Y (2019) Study on the influence of surface potential on the nitrate adsorption capacity of metal modified biochar. Environ Sci Pollut Res 26:3065–3074. https://doi.org/10.1007/s11356-018-3815-z
Lu N, Oza S (2013) Thermal stability and thermo-mechanical properties of hemp-high density polyethylene composites: Effect of two different chemical modifications. Compos B Eng 44(1):484–490. https://doi.org/10.1016/j.compositesb.2012.03.024
Maleki A, Mahvi AH, Ebrahimi R, Jamil Khan JK (2010) Evaluation of barley straw and its ash in removal of phenol from aqueous system. World Appl Sci J 8(3):369–373
Min L, Zhongsheng Z, Zhe L, Haitao W (2020) Removal of nitrogen and phosphorus pollutants from water by FeCl3-impregnated biochar. Ecol Eng 149:105792. https://doi.org/10.1016/j.ecoleng.2020.105792
Mo J, Yang Q, Zhang N, Zhang W, Zheng Y, Zhang Z (2018) A review on agro-industrial waste (AIW) derived adsorbents for water and wastewater treatment. J Environ Manage 227:395–405. https://doi.org/10.1016/j.jenvman.2018.08.069
Mohan D, Kumar H, Sarswat A, Alexandre-Franco M, Pittman Jr CU (2014) Cadmium and lead remediation using magnetic oak wood and oak bark fast pyrolysis biochars. Chem Eng J 236:513–528. https://doi.org/10.1016/j.cej.2013.09.057
Nguyen TAH, Ngo HH, Guo WS, Nguyen TV, Zhang J, Liang S, Nguyen NC (2014) A comparative study on different metal loaded soybean milk by-product 'okara' for biosorption of phosphorus from aqueous solution. Bioresour Technol 169:291–298. https://doi.org/10.1016/j.biortech.2014.06.075
Nguyen TH, Pham TH, Nguyen T, Hong T, Nguyen TN, Nguyen MV, Tran Dinh T, Nguyen MP, Do TQ, Phuong T, Hoang TT, Mai Hung TT, Thi VHT (2019) Synthesis of iron-modified biochar derived from rice straw and its application to arsenic removal. J Chem 5295610. https://doi.org/10.1155/2019/5295610
Nijboer RC, Verdonschot PF (2004) Variable selection for modelling effects of eutrophication on stream and river ecosystems. Ecol Modell 177:17–39. https://doi.org/10.1016/j.ecolmodel.2003.12.050
Ou W, Lan X, Guo J, Cai A, Liu P, Liu N, Lei Y (2023) Preparation of iron/calcium-modified biochar for phosphate removal from industrial wastewater. J Clean Prod 383:135468. https://doi.org/10.1016/j.jclepro.2022.135468
Parker HL, Hunt AJ, Budarin VL, Shuttleworth PS, Miller KL, Clark JH (2012) The importance of being porous: polysaccharide-derived mesoporous materials for use in dye adsorption. RSC Adv 2(24):8992–8997. https://doi.org/10.1039/c2ra21367b
Perera GN, Rojas DT, Hoepker SN, Olsen G, Craggs R, Hartland A (2024) Iron− based composites for in− field phosphorus removal from agricultural drainage. Surf Interfaces 51:104566. https://doi.org/10.1016/j.surfin.2024.104566
Perera MGN, Galagedara YR, Ren Y, Jayaweera M, Zhao Y, Weerasooriya R (2018) Fabrication of fullerenol-incorporated thin-film nanocomposite forward osmosis membranes for improved desalination performances. J Polym Res 25(9). https://doi.org/10.1007/s10965-018-1593-4
Ramírez-Montoya LA, Hernández-Montoya V, Montes-Morán MA (2014) Optimizing the preparation of carbonaceous adsorbents for the selective removal of textile dyes by using Taguchi methodology. J Anal Appl Pyrolysis 109:9–20. https://doi.org/10.1016/j.jaap.2014.07.018
Sedmihradská A, Pohořelý M, Jevič P, Skoblia S, Beňo Z, Farták J, ... Hartman M (2020) Pyrolysis of wheat and barley straw. Res Agric Eng 66(1). https://doi.org/10.17221/26/2019-RAE
Sembiring S, Simanjuntak W, Manurung P, Asmi D, Low IM (2014) Synthesis and characterisation of gel-derived mullite precursors from rice husk silica. Ceram Int 40(5):7067–7072. https://doi.org/10.1016/j.ceramint.2013.12.038
Usman AR, Ahmad M, El-Mahrouky M, Al-Omran A, Ok YS, Sallam AS, Al-Wabel MI (2016) Chemically modified biochar produced from conocarpus waste increases NO3- removal from aqueous solutions. Environ Geochem Health 38:511–521. https://doi.org/10.1007/s10653-015-9736-6
Vaughn SF, Kenar JA, Tisserat B, Jackson MA, Joshee N, Vaidya BN, Peterson SC (2017) Chemical and physical properties of Paulownia elongata biochar modified with oxidants for horticultural applications. Ind Crop Prod 97:260–267. https://doi.org/10.1016/j.indcrop.2016.12.017
Wang F, Ren X, Sun H, Ma L, Zhu H, Xu J (2016) Sorption of polychlorinated biphenyls onto biochars derived from corn straw and the effect of propranolol. Bioresour Technol 219:458–465. https://doi.org/10.1016/j.biortech.2016.08.006
Wang Z, Nie E, Li J, Yang M, Zhao Y, Luo X, Zheng Z (2012) Equilibrium and kinetics of adsorption of phosphate onto iron-doped activated carbon. Environ Sci Pollut Res 19:2908–2917. https://doi.org/10.1007/s11356-012-0799-y
Ward MH (2009) Too much of a good thing? Nitrate from nitrogen fertilizers and cancer. Rev Environ Health 24(4):357–363. https://doi.org/10.1515/REVEH.2009.24.4.357
Xie B, Zuo J, Gan L, Liu F, Wang K (2014) Cation exchange resin supported nanoscale zero-valent iron for removal of phosphorus in rainwater runoff. Front Environ Sci Eng 8:463–470. https://doi.org/10.1007/s11783-013-0575-3
Yan B, Niu CH (2018) Adsorption behavior of norfloxacin and site energy distribution based on the Dubinin-Astakhov isotherm. Sci Total Environ 631:1525–1533. https://doi.org/10.1016/j.scitotenv.2018.03.119
Yan B, Niu CH, Wang J (2017) Analyses of levofloxacin adsorption on pretreated barley straw with respect to temperature: kinetics, π–π electron-donor–acceptor interaction and site energy distribution. Environ Sci Technol 51(14):8048–8056. https://doi.org/10.1021/acs.est.7b00327
Yang Q, Wang X, Luo W, Sun J, Xu Q, Chen F, Zhao J, Wang S, Yao F, Wang D, Li X, Zeng G (2018) Effectiveness and mechanisms of phosphate adsorption on iron-modified biochars derived from

waste activated sludge. Bioresour Technol 247:537–544. https://doi.org/10.1016/j.biortech.2017.09.136

Yue Y, Yu Z, Yue X, Zhou W, Wang S, Yang Y, Wang S (2024) Activated carbon derived from highland barley straw for removing heavy metals and organic pollutants. Int J Low-Carbon Technol 19:135–141. https://doi.org/10.1093/ijlct/ctad042

Zheng Y, Zimmerman AR, Gao B (2020) Comparative investigation of characteristics and phosphate removal by engineered biochars with different loadings of magnesium aluminum or iron. Sci Total Environ 747:141277. https://doi.org/10.1016/j.scitotenv.2020.141277

Zhu Z, Toor SS, Rosendahl L, Yu D, Chen G (2015) Influence of alkali catalyst on product yield and properties via hydrothermal liquefaction of barley straw. Energy 80:284–292. https://doi.org/10.1016/j.energy.2014.11.071